Particle nucleation in a forested environment

Nallathamby, Punith D.

2014-10

Nallathamby , P D , Hopke , P K , Rossner , A , Dhaniyala , S , Marzocca , P , Petäjä , T , Barthelmie , R J & Pryor , S C 2014 , ' Particle nucleation in a forested environment ' , Atmospheric pollution research , vol. 5 , no. 4 , pp. 805-810 . https://doi.org/10.5094/APR.2014.090

http://hdl.handle.net/10138/224175
https://doi.org/10.5094/APR.2014.090

Atmospheric Pollution Research 5 (2014) 805-810

Atmospheric Pollution Research

www.atmospolres.com

Particle nucleation in a forested environment

Punith D. Nallathamby [1], Philip K. Hopke [1], Alan Rossner [1], Suresh Dhaniyala [1], Piergiovanni Marzocca [1], Tuukka Petaja [2], Rebecca J. Barthelmie [3], Sara C. Pryor [3]

[1] *Center for Air Resources Engineering and Science, Clarkson University, Potsdam, NY 13699*
[2] *Department of Physics, University of Helsinki, Helsinki, Finland*
[3] *Atmospheric Science Program, College of Arts and Sciences, Indiana University, Bloomington, IN 47405, USA*

ABSTRACT

Atmospheric nucleation is now recognized to be an important source of ambient particles. In this study, ground–based measurements using a tower were used to observe new particle formation in the Morgan Monroe State Forest (MMSF) in Southwestern Indiana in May 2008. Nucleation was observed at MMSF on a number of days through examination of the particle size distributions. Most of these events were nucleation and growth events that are typical of regional nucleation phenomena. The particle size and sulfuric acid concentration data were used to investigate the mechanism for the observed nucleation events. Four of the ten observed nucleation events were clearly the result of activation of pre–existing clusters. The others seem likely to be the result of classical ternary nucleation.

Keywords: *Nucleation, particle concentrations, particle size distributions, sulfuric acid*

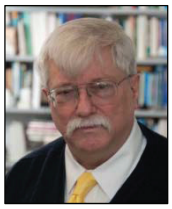

Corresponding Author:
Philip K. Hopke
☎ : *+1-315-268-3861*
🖷 : *+1-315-268-4410*
✉ : *hopkepk@clarkson.edu*

Article History:
Received: 06 March 2014
Revised: 18 June 2014
Accepted: 18 June 2014

doi: 10.5094/APR.2014.090

1. Introduction

Atmospheric particles interact with radiation to influence the energy balance of the atmosphere and thus directly influence the climate (Koloutsou–Vakakis et al., 1998; IPCC, 2007) and reduce visibility (Malm, 1999). Via their interaction with radiation, particles also have a direct influence on the terrestrial carbon sink (Moffat et al., 2010). Particles with diameters larger than ~0.2 µm serve as cloud condensation nuclei and are essential for cloud formation and dictate the cloud albedo, thus also influence climate via indirect forcing (IPCC, 2007; Kazil et al., 2010). Further, exposure to elevated concentrations of particles causes breathing disorders and cardiovascular disease (Donaldson et al., 2002; Pope et al., 2002). Because of their varied effects on visibility, health, cloud formation and climate, it is important for us to understand and learn as to how to model their behavior.

Nucleation is a key source of atmospheric particle number and results in the formation of new particles in the size range of 1 nm to 3 nm (Holmes, 2007; Kulmala and Kerminen, 2008; Nieminen et al., 2009). Temperature, humidity, surface area and age of existing aerosol and ambient gas phase concentrations are some of the factors on which the rate of heterogeneous nucleation depends (Kulmala et al., 2004). These particles either coagulate or other vapors condense on them to form larger particles. The rate at which these particles grow is dependent on factors such as the initial particle size, chemical composition, concentration, temperature and vapor pressure of condensing substance. Loss of particles occurs by deposition of the particles to the surface (Pryor et al., 2008), precipitation scavenging (Flossmann and Wobrock, 2010), and evaporation of the particle (Leong et al., 1983). To further develop atmospheric models on the regional and global scales, it is important to incorporate atmospheric nucleation because of its role in determining particle concentration and size distributions.

There is limited information currently available regarding the mechanisms of nucleation events. The Nucleation In ForesTs (NIFTy) campaign was held at the Morgan Monroe State Forest (MMSF) during May 2008 (Pryor et al., 2011). Nucleation events can be thermodynamically limited (classical ternary nucleation) or they can occur through the activation of pre–existing clusters. Examining the details of individual events permits the assignment of the primary nature of the events. Nucleation events are often related to the breakup of the night–time stable layer. The main objectives of this analysis of the data from the NIFTy campaign are to identify the principal mechanisms of nucleation and to explore the link between nucleation and the breakdown of nocturnal boundary layer.

2. Instrumentation and Methodology

2.1. Instruments used

The NIFTy campaign was conducted during May 2008 and is described in detail by Pryor et al. (2011). May was chosen for the intensive study based on the long–term particle size distribution measurements that indicated that the highest frequency of nucleation occurred in May (Pryor et al., 2010). Below we describe

only a sub–set of the instrumentation from which data are used herein. The locations of the sampling sites are presented in Figure 1.

Continuous particle size distribution measurements are taken on a 46 m tower located in the MMSF in Southern Indiana at 39°19'23.63"N and 86°24'48.04"W. As part of these continuous measurements, a Fast Mobility Particle Sizer (FMPS, TSI Model 3091) (Mirme and Tamm, 1991; Mirme and Tamm, 1993; Tammet et al., 2002) at the bottom of the tower measures particle concentrations from the top of the tower using a 3.175 cm diameter copper tube (Pryor et al., 2010). The FMPS measures size distributions from 5.6 to 560 nm with a time resolution of 1 second. Corrections were made to the readings for tubing losses (Pryor et al., 2010). The ongoing measurements were supplemented with two CPC's (TSI Model 3781) deployed near the canopy; one at 30 m (CPC1) and the other at 15 m (CPC2) from the base of the tower. These water–based condensation particle counters (CPC, TSI Model 3781) have a 50% counting efficiency at 6 nm. The measurements made using the FMPS and CPCs were averaged to a time resolution of 1 minute. Micro–meteorological measurements are taken from the top of the tower, along with a ceilometer. A tethersonde, ceilometer, and Doppler Light Detection and Ranging (LIDAR) were deployed in an open location near the tower to study the planetary boundary layer (Pryor et al., 2011). Measurements of SO_2 concentrations were made at the tower site using a standard monitor (Thermo Model 43c). Sulfuric acid concentrations were measured using a Chemical Ionization Mass Spectrometer (Berresheim et al., 2000).

Sulfur dioxide and sulfuric acid measurements were made at the base of the tower. Sulfur dioxide and sulfuric acid were continuously measured at 10 second and 30 minute intervals, respectively.

3. Results and Discussion

3.1. Particle nucleation events

During the NIFTy campaign, FMPS data were successfully collected on 22 days from the top of the tower. Of these 22 days, nucleation events were detected on 13 days. Nucleation events can be of two types (Jeong et al., 2004; Stanier et al., 2004). Regional nucleation events are characterized by a burst of small particles (6 to 20 nm) that then grow into 60 to 80 nm particles. These events have a characteristic banana shape in the plots of size distributions as a function of time. The other type of event is a plume event in which a burst of small particles (<20 nm) without subsequent growth. However, complete data were only available for 10 events. Since nucleation occurs in the size range of 1–3 nm and the instrument's lower detection limit is 5.6 nm for the FMPS and 6 nm for the CPCs, the initial portion of the nucleation events where the newly formed particle sizes are smaller than 5.6 nm cannot be observed. However, the growth patterns once they grow to 5.6 nm can be observed.

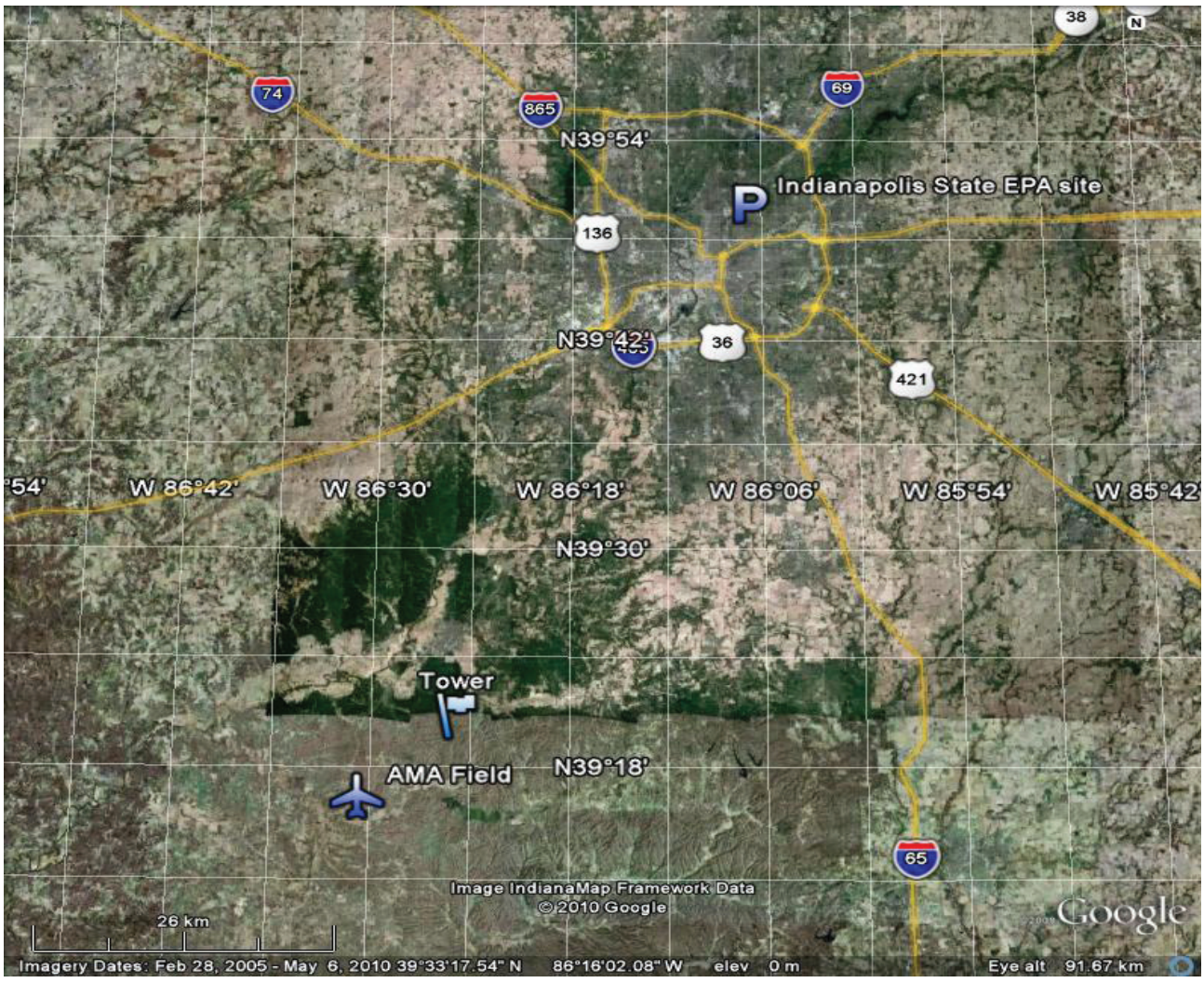

Figure 1. *Satellite view of Southwestern Indiana showing the sampling locations.*

Figure 2 shows contour plots of the FMPS data on May 17th collected from the tower. Figure 2 shows that at around 10:00 am, there was a sudden increase in particles in the lower size ranges. As time proceeds, it is seen that these particles grow in size with a slight drop in concentration. This behavior is a typical banana–shaped curve indicating a regional nucleation with growth has occurred (Jeong et al., 2004; Stanier et al., 2004). As the particles grow, the decrease in concentration is due to deposition and coagulation of particles. Gradually, particle concentrations decrease and become indistinguishable from background concentrations. A particle budget analysis was described by Pryor et al. (2011). Based on the aerosol budget analysis, they report an entrainment velocity of 7 cm s^{-1}. This result is in good agreement with the LIDAR estimate of mean vertical velocities (in the period 14:00 to 14:30 at 300 m) of −8 cm s^{-1}. The negative number indicates a downwards vertical velocity.

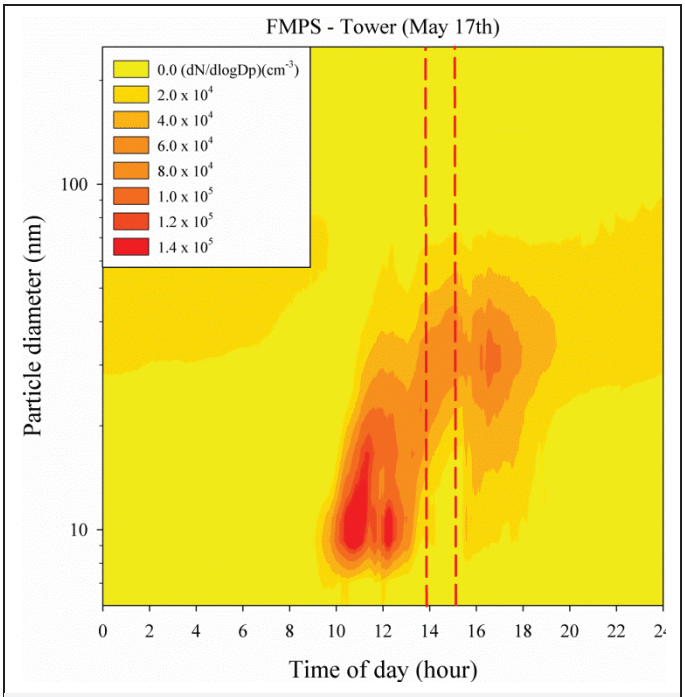

Figure 2. *Contour plot of FMPS data from the tower in MMSF on May 17, 2008.*

Similar nucleation events in the MMSF can be observed on May 19th and 22nd as seen in Figures S1 and S2, respectively (see the Supporting Material, SM). From these contour plots, it is evident that nucleation occurred. On May 19th, a sudden increase in small particles (<10 nm) was noticed, but the subsequent growth forming a banana–shaped curve was not observed. This result could be explained by a sudden change in wind direction. Initially, the wind was blowing from the west, and at around 1:00 pm, the wind started blowing from the northeast. The change in wind direction and the accompanying precipitation resulted in the break in the growth pattern.

3.2. Classification of nucleation events

Nucleation events can be classified in several different ways. Dal Maso et al. (2005) classify nucleation events into three classes based on the size of the initially observed particles and their subsequent growth to larger sizes. In a class A event, the formation of particles with number geometric mean diameter below 25 nm is clearly followed by growth. In a class B event, the formation stage of the new particles is not clearly visible; but the growth stage is observed. In a class C event, the formation stage of new particles is observed by an increase in the ultra–fine particles. However, there is no growth stage following the nucleation event. Table 1 gives a summary of nucleation event classes observed at the MMSF tower during the campaign.

Table 1. *Nucleation event classification and strength*

Date	Event Classification	
	Dal Maso et al. Class	Stanier et al. Class
May 12th	A	Moderate
May 13th	C	Moderate
May 16th	A	Moderate
May 17th	C	Strong
May 18th	C	Moderate
May 19th	A	Strong
May 20th	A	Weak
May 21st	A	Moderate
May 22nd	A	Moderate
May 24th	A	Weak
May 25th	A	Moderate
May 27th	A	Weak

The nucleation events were also classified as strong, moderate and weak (Stanier et al., 2004) based on the net rate of increase in particles in the bin size 8.04 nm (from now on referred to as N_8). This size is chosen since it is really the first size range that is well measured by the FMPS. The classification was made as follows: if $dN_8/dt>10\ 000\ cm^3\ h^{-1}$, then the nucleation event was classified as strong. If $4\ 000<dN_8/dt<10\ 000\ cm^3\ h^{-1}$, then classified as moderate. And if $dN_8/dt<4\ 000\ cm^3\ h^{-1}$, it was classified as weak. A summary of the strength of the nucleation events at MMSF is given in Table 1. Figure 2 shows an example of strong nucleation.

3.3. Nucleation mechanisms

The atmosphere contains a mixture of pre–existing particles, moisture, molecular and ionic clusters, and volatile organic compounds that are may be anthropogenic and biogenic in origin. The composition of this atmospheric mixture varies from one location to another, whether an urban environment, a coastal region, or a forest etc. Variation in atmospheric composition, coupled with different meteorological conditions, affords a variety of mechanisms to produce nucleation. The most common forms of atmospheric nucleation are (Kulmala and Kerminen, 2008):

(1) homogeneous binary water–sulfuric acid nucleation
(2) homogeneous ternary water–sulfuric acid–ammonia nucleation
(3) ion–induced nucleation
(4) barrier–less or kinetically controlled homogeneous nucleation

Of these, it was hypothesized that nucleation involving sulfuric acid was most likely to occur under the conditions of the NIFTy study than nucleation of secondary organic compounds given the known upwind proximity of coal–fired power plants that would supply significant quantities of SO_2.

The NIFTy campaign data was analyzed following the approach of Sihto et al. (2006). Because nucleation typically occurs to produce particles smaller than the detection systems used to measure the particle size distributions, Sihto et al. (2006) developed an approach that assumes that the number of particles and the growth rate at the lowest measureable particle size can be used to estimate the nucleation rates. They derived a set of equations for particles in the 3 to 6 nm range. For the measurements made in the NIFTy campaign, the equations were modified to use the measured particle concentrations in the 6 to 8 nm

range. The particle number concentration in the 6 nm range (N_6) was plotted along with delayed $[H_2SO_4]^{n_{N_6}}$. Figures 3 and S4 (see the SM) show the data measured on May 19th and May 22nd, respectively. The time delay Δt_{N_6} was varied in increments of 10 minutes, and the exponent n_{N_6} was varied from 0 to 100 in increments of 0.01. Prior work had tested a limited range of exponents. However, there was no theoretical basis for limiting the exponent since the objective is to provide a best predicted value. The combination of the two parameters that resulted in the highest correlation coefficient between the variables, r_{max}, was used. The resulting Δt_{N_6} value was used to calculate the growth rate using:

$$GR_{1-6} = \frac{6\ nm - 1\ nm}{\Delta t_{N_6}} = \frac{5\ nm}{\Delta t_{N_6}} \quad (1)$$

The growth rate is assumed to be the same for the entire event. From the estimated growth rate, the formation rate of 6 nm particles (J_6) was estimated by:

$$J_6 = \frac{dN_6}{dt} + CoagS_6 . N_6 + \frac{1}{2\ nm} GR . N_6 \quad (2)$$

where, $CoagS_6$ is the coagulation sink for 6 nm particles.

$$J_1(t) = J_6(t') . exp\left(\gamma \frac{CS'}{GR_{1-6}} \left(\frac{1}{1\ nm} - \frac{1}{6\ nm}\right)\right) \quad (3)$$

where, CS' is the condensational sink in m^{-2}, t' is $t + \Delta t_{N_6}$ and γ is a coefficient with a value of about 0.23 $m^2\ nm^2\ h^{-1}$ (Sihto et al., 2006). The value of J_6 is substituted in Equation (3) to get the value of formation rate of 1 nm particles (J_1).

The J_1 values were then plotted against $[H_2SO_4]^{n_{J_1}}$. The best fit was obtained by varying the exponent n_{J_1}. Depending upon the value of n_{J_1}, the predominant nucleation mechanism for that day was determined (Sihto et al., 2006). Therefore, only values of n_{J_1}=1, 2, and 3 were used to find the best fit. Figures 4 and S5 (see the SM) are prepared with J_1 and sulfuric acid concentration with the fitted power of n_{J_1} on May 19th and May 22nd, respectively.

Table 2 summarizes the exponent values, n_{N_6} and n_{J_1}, the time delay Δt_{N_6}, and the growth rate from 1 to 6 nm. Not all of the correlation coefficients were statistically significant. The significant values are shown in bold font. For six of event days, the value of n_{J_1} was 3. However, none of the correlation coefficients on these days were statistically significant and thus, the assignment of the exponent is uncertain. For four days with three of them showing statistically significant correlation coefficients, the n_{J_1} value was 1. The remaining correlation was marginally significant with a probability of 0.095. A value of n_{J_1} equal to 3 indicates that the atmospheric nucleation event was thermodynamically limited (classical ternary nucleation). A value of 1 suggests that activation of pre–existing clusters is dominant. It is seen that during the NIFTy campaign in May 2008, the most clearly defined process was nucleation by cluster activation.

3.4. Nocturnal Boundary Layer (NBL)

Pryor et al. (2011) show a clear link between the erosion of a stable boundary layer and the onset of the nucleation events. Estimations of the hourly mixed layer heights across the NIFTy campaign period are provided in Table S1 (see the SM). For the days with Class A events (Table 1), the composite of LIDAR derived wind speeds, turbulence intensities, and vertical velocities show a clear transition from a strongly stratified atmosphere to a much weaker vertical gradient of wind speed, increased turbulence intensities, and stronger downward velocities that are consistent with the growth of the mixed layer and entrainment of air from the residual layer (See Figure 10 in Pryor et al., 2010). These transitions occur about 1 hour prior to the onset of the nucleation events.

4. Conclusions

In the NIFTy campaign conducted during May 2008, measurements were made successfully for 22 days at MMSF. Nucleation was observed on 13 days at MMSF. From the estimated growth rate (from 1 to 6 nm) for each day, it was found that the clearly observable nucleation mechanism was consistent with cluster activation. The events are other days appear to be the result of classical ternary nucleation, but the data for all of these events could not be fit with a statistically significant result. The onset of nucleation occurred after the breakdown of the nocturnal boundary layer in agreement with other studies.

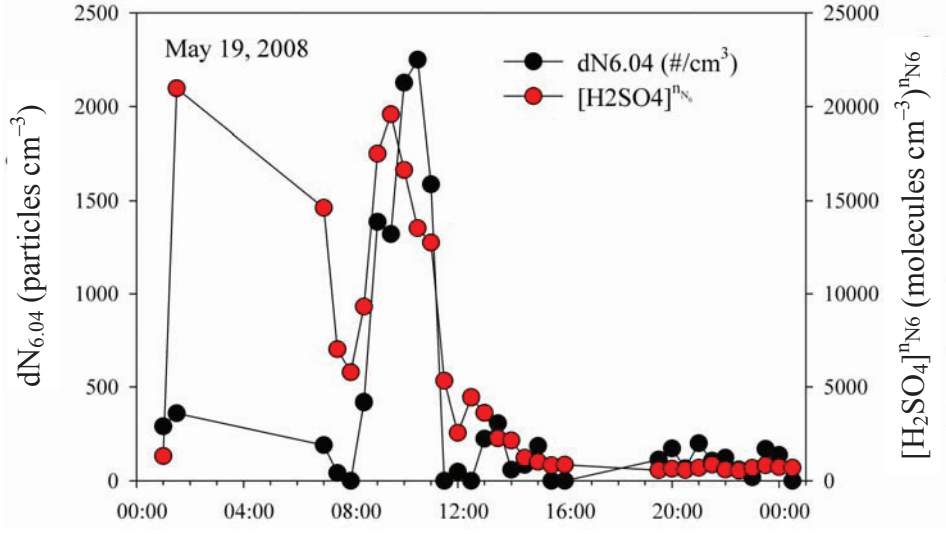

Figure 3. *The number concentration of 6 nm particles and time delayed sulfuric acid concentration with the fitted time lag of Δt_{N_6} and n_{N_6} at the MMSF tower on May 19th.*

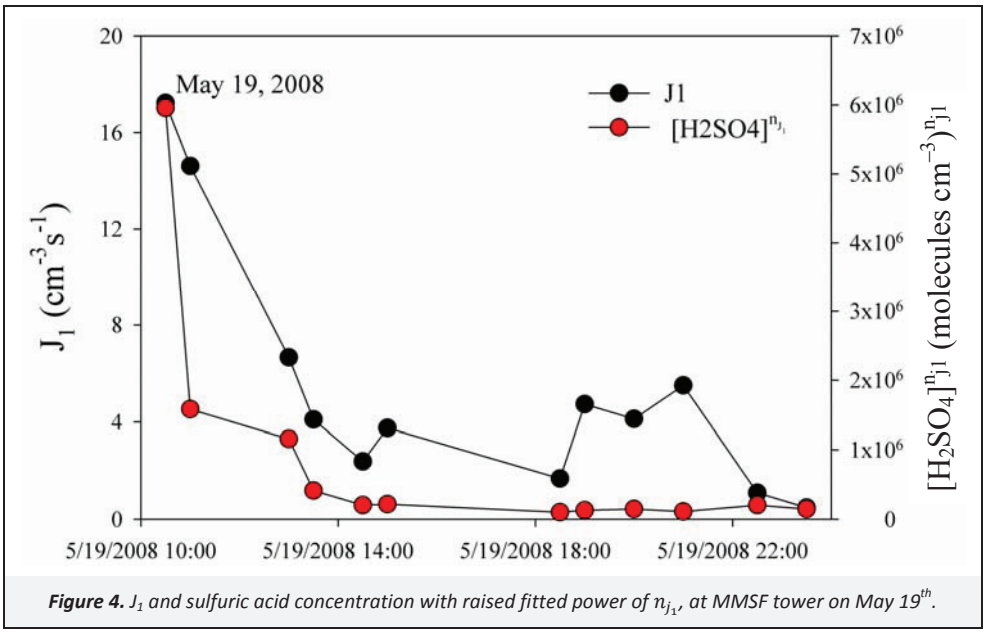

Figure 4. *J_1 and sulfuric acid concentration with raised fitted power of n_{j_1}, at MMSF tower on May 19th.*

Table 2. *Summary of exponent values n_{N_6} and n_{j_1}, time delay Δt_{N_6}, and growth rate from 1 to 6 nm*

Date	n_{N_6}	Δt_{N_6} (hours)	GR (nm/h)	n_{j_1}	Correlation Coefficients		
					n_{j_1}=1	n_{j_1}=2	n_{j_1}=3
17–May	20.3	1.0	5.0	1	**0.314**	0.187	0.115
18–May	1.4	1.5	3.3	3	–0.016	0.009	0.027
19–May	0.6	1.5	3.3	1	**0.340**	0.278	0.199
20–May	22.0	0.5	10.0	3	–0.106	–0.073	–0.058
21–May	8.6	1.0	5.0	1	0.127	0.103	0.055
22–May	2.2	1.5	3.3	1	0.212	0.165	0.123
24–May	21.4	3.5	1.4	3	–0.198	–0.121	–0.099
25–May	21.4	1.5	3.3	3	–0.034	–0.015	–0.004
27–May	0.0	0.5	10.0	1	0.032	–0.061	–0.090
29–May	0.0	3.5	1.4	1	**0.728**	0.701	0.627

The significant values are shown in bold font

Acknowledgments

This work was supported by National Science Foundation Grant 0544745 and supplement. The ceilometers and micro meteorological data used herein were collected under funding from the Office of Science (BER), U.S. Department of Energy, grant DE–FG02–07ER64371 (D. Dragoni et al., principal investigators). Technical support from Steve Scott, and the field assistance of M. Brothers, J. Butler, W. Hull, L. Mauldin III, H. Porter, E. Riley A. Spaulding, D. Valyou, D. Young and E. Zito is gratefully acknowledged. We also gratefully acknowledge the efforts of T. Jobson, and the assistance of both the members of the Monroe County Radio Control Club and the Indiana Department of Environmental Management. The authors gratefully acknowledge the NOAA Air Resources Laboratory (ARL) for the provision of the HYSPLIT transport and dispersion model and/or READY website (http://www.arl.noaa.gov/ready.php) used in this publication.

Supporting Material Available

Contour plot of FMPS data from the tower in MMSF on May 19th (Figure S1), Contour plot of FMPS data from the tower in MMSF on May 22nd (Figure S2), Comparison of N_8 and N_{22} concentrations at MMSF and Indianapolis on May 19th (Figure S3), The number concentration of 6 nm particles and delayed sulfuric acid concentrations with the fitted time lag of Δt_{N_6} and raised to the fitted power of n_{N_6}at the MMSF tower on May 22nd (Figure S4), J_1 and sulfuric acid concentrations with raised fitted power of n_{J_1}, at MMSF tower on May 22nd (Figure S5), Estimation of mixed layer height in meters above ground level for each day during the NIFTy campaign (Table S1). This information is available free of charge via the internet at http://www.atmospolres.com.

References

Berresheim, H., Elste, T., Plass–Dulmer, C., Eisele, F.L., Tanner, D.J., 2000. Chemical ionization mass spectrometer for long–term measurements of atmospheric OH and H_2SO_4. *International Journal of Mass Spectrometry* 202, 91–109.

Dal Maso, M., Kulmala, M., Riipinen, I., Wagner, R., Hussein, T., Aalto, P.P., Lehtinen, K.E.J., 2005. Formation and growth of fresh atmospheric aerosols: Eight years of aerosol size distribution data from SMEAR II, Hyytiala, Finland. *Boreal Environment Research* 10, 323–336.

Donaldson, K., Brown, D., Clouter, A., Duffin, R., MacNee, W., Renwick, L., Tran, L., Stone, V., 2002. The pulmonary toxicology of ultrafine particles. *Journal of Aerosol Medicine–Deposition Clearance and Effects in the Lung* 15, 213–220.

Flossmann, A.I., Wobrock, W., 2010. A review of our understanding of the aerosol–cloud interaction from the perspective of a bin resolved cloud scale modelling. *Atmospheric Research* 97, 478–497.

Holmes, N.S., 2007. A review of particle formation events and growth in the atmosphere in the various environments and discussion of mechanistic implications. *Atmospheric Environment* 41, 2183–2201.

IPCC (Intergovernmental Panel on Climate Change), 2007. Climate Change 2007: Synthesis Report Summary for Policymakers, Cambridge University Press, Cambridge, U.K., 23 pages.

Jeong, C.H., Hopke, P.K., Chalupa, D., Utell, M., 2004. Characteristics of nucleation and growth events of ultrafine particles measured in Rochester, NY. *Environmental Science & Technology* 38, 1933–1940.

Kazil, J., Stier, P., Zhang, K., Quaas, J., Kinne, S., O'Donnell, D., Rast, S., Esch, M., Ferrachat, S., Lohmann, U., Feichter, J., 2010. Aerosol nucleation and its role for clouds and earth's radiative forcing in the aerosol–climate model ECHAM5–HAM. *Atmospheric Chemistry and Physics* 10, 10733–10752.

Koloutsou–Vakakis, S., Rood, M.J., Nenes, A., Pilinis, C., 1998. Modeling of aerosol properties related to direct climate forcing. *Journal of Geophysical Research–Atmospheres* 103, 17009–17032.

Kulmala, M., Kerminen, V.M., 2008. On the formation and growth of atmospheric nanoparticles. *Atmospheric Research* 90, 132–150.

Kulmala, M., Laakso, L., Lehtinen, K.E.J., Riipinen, I., Dal Maso, M., Anttila, T., Kerminen, V.M., Horrak, U., Vana, M., Tammet, H., 2004. Initial steps of aerosol growth. *Atmospheric Chemistry and Physics* 4, 2553–2560.

Leong, K.H., Hopke, P.K., Stukel, J.J., 1983. Evaporative mass losses from particle samples. *Journal of Aerosol Science* 14, 611–613.

Malm, W.C., 1999. Introduction to Visibility, http://vista.cira.colostate.edu/improve/Education/intro_to_visibility.pdf, accessed in June 2014.

Mirme, A., Tamm, E., 1993. 20 P 04 Electric aerosol spectrometer. Calibration and error account. *Journal of Aerosol Science* 24, S211–S212.

Mirme, A., Tamm, E., 1991. Comparison of sequential and parallel measurement principles in aerosol spectrometry. *Journal of Aerosol Science* 22, S331–S334.

Moffat, A.M., Beckstein, C., Churkina, G., Mund, M., Heimann, M., 2010. Characterization of ecosystem responses to climatic controls using artificial neural networks. *Global Change Biology* 16, 2737–2749.

Nieminen, T., Manninen, H.E., Sihto, S.L., Yli–Juuti, T., Mauldin, R.L., Petaja, T., Riipinen, I., Kerminen, V.M., Kulmala, M., 2009. Connection of sulfuric acid to atmospheric nucleation in Boreal Forest. *Environmental Science & Technology* 43, 4715–4721.

Pope, C.A., Burnett, R.T., Thun, M.J., Calle, E.E., Krewski, D., Ito, K., Thurston, G.D., 2002. Lung cancer, cardiopulmonary mortality, and long–term exposure to fine particulate air pollution. *JAMA–Journal of the American Medical Association* 287, 1132–1141.

Pryor, S.C., Barthelmie, R.J., Sorensen, L.L., McGrath, J.G., Hopke, P., Petaja, T., 2011. Spatial and vertical extent of nucleation events in the Midwestern USA: Insights from the Nucleation in ForesTs (NIFTy) experiment. *Atmospheric Chemistry and Physics* 11, 1641–1657.

Pryor, S.C., Spaulding, A.M., Barthelmie, R.J., 2010. New particle formation in the Midwestern USA: Event characteristics, meteorological context and vertical profiles. *Atmospheric Environment* 44, 4413–4425.

Pryor, S.C., Gallagher, M., Sievering, H., Larsen, S.E., Barthelmie, R.J., Birsan, F., Nemitz, E., Rinne, J., Kulmala, M., Groenholm, T., Taipale, R., Vesala, T., 2008. A review of measurement and modelling results of particle atmosphere–surface exchange. *Tellus Series B–Chemical and Physical Meteorology* 60, 42–75.

Sihto, S.L., Kulmala, M., Kerminen, V.M., Dal Maso, M., Petaja, T., Riipinen, I., Korhonen, H., Arnold, F., Janson, R., Boy, M., Laaksonen, A., Lehtinen, K.E.J., 2006. Atmospheric sulphuric acid and aerosol formation: Implications from atmospheric measurements for nucleation and early growth mechanisms. *Atmospheric Chemistry and Physics* 6, 4079–4091.

Stanier, C.O., Khlystov, A.Y., Pandis, S.N., 2004. Nucleation events during the Pittsburgh Air Quality Study: Description and relation to key meteorological, gas phase, and aerosol parameters. *Aerosol Science and Technology* 38, 253–264.

Tammet, H., Mirme, A., Tamm, E., 2002. Electrical aerosol spectrometer of Tartu University. *Atmospheric Research* 62, 315–324.